Kinetics in sub-barrier fusion of spherical nuclei

V. N. Kondratyev,[1,*] A. Bonasera,[2] and A. Iwamoto[3]
[1]*Advanced Science Research Center, Japan Atomic Energy Research Institute, Tokai, Naka, Ibaraki 319-1195, Japan*
[2]*Laboratorio Nazionale del Sud, INFN, v. S. Sofia 44, 95125 Catania, Italy*
[3]*Department of Materials Science, Japan Atomic Energy Research Institute, Tokai, Naka, Ibaraki 319-1195, Japan*
(Received 14 May 1999; published 22 March 2000)

The semiclassical transport theory is applied to the description of heavy-ion fusion at energies below and above the Coulomb barrier. The paths connecting entrance and exit fusion reaction channels are found as a continuous solution of the Vlasov transport equation in classically allowed and forbidden regions associated with suitably defined collective variables. The effects of nuclear deformation, neck formation, and nonlocality are quantified on the basis of microscopic simulations and analyzed. The results of calculations give good fits to experimental data for fusion of nearly symmetric oxygen and nickel isotope pairs.

PACS number(s): 25.70.Jj, 25.60.Dz, 21.30.−x, 25.60.Je

I. INTRODUCTION

The problem of the tunneling of a many-body system appears in many branches of physics ranging from quantum (chemical) processes in molecules and solids [1] to star evolution (cf. [2,3]). Detailed information regarding such an effect is provided by studies of heavy-ion sub-barrier fusion phenomena. For heavy nuclei the experimental measurements commonly yield a surprisingly large fusion cross section, several orders of magnitude larger as compared to respective evaluations obtained with the WKB approximation (see [4–7] and references therein). Consequently, a number of models based on a macroscopic parametrization of heavy-ion collision processes have been proposed for the description of such a dramatic reinforcement of the fusion channel at sub-barrier energies. Such models usually account for a coupling of translational motion of nuclei to the degrees of freedom associated with other competing reaction channels, like excitations of target and/or projectile, nucleon transfer, nucleus polarization and deformation, and multidimensional tunneling. The applications of the coupled-channel treatment have been very successful in understanding some mechanisms of experimentally observed enhancement for light and asymmetric systems in the vicinity of the barrier top [5,7–9]. The difficulty of coupled channel calculations of fusion cross sections increases in a dramatic way for the cases of heavy systems and at deeply sub-barrier collisions because of a large number and the complexity of possible channels. At beam energies much below the barrier the experimentally observed enhancement can be properly reproduced by including nonlocal effects [10–13] and considering thereby a distance dependent effective mass of translational motion [14]. The models with a nonlocal nucleus-nucleus interaction are successfully applied for the description of other reaction channels as well (cf. [15]). Starting from the reduced mass for well-separated nuclei the effective mass decreases with decreasing internuclear distance within such a model. It is worth noticing that introducing an effective mass is a familiar procedure in studies of nuclear fission (i.e., an inverted process to fusion). However, the fission systematics suggests a large effective mass at small distances, up to an order of magnitude larger than the reduced mass (cf. [16–18]). This qualitative difference in fusion and fission phenomena seems to indicate the significance of nonadiabatic features in a fusion reaction, often presumed to be negligible (cf. [19]).

In this paper we discuss some attempts towards a better understanding of specific properties of sub-barrier fusion within the framework of a mean-field transport theory. Significant progress towards the realization of such a treatment at above-barrier energies has been made by applying the transport equations of the time-dependent Hartree-Fock (TDHF) type and its semiclassical counterparts based, e.g., on the Wigner formalism for nuclear dynamics [20–24]. As a matter of fact this type of approach represents the semiclassical limit of collective nuclear dynamics. Making use of this feature the mean-field treatment can be extended by employing the Feynman path-integral technique in order to describe, e.g., sub-barrier fusion reactions. For instance, within the framework of recently proposed method [25–27] the path connecting, e.g., the entrance and exit fusion reaction channels is found as a continuous solution of the Vlasov mean-field equation of motion in classically allowed and forbidden regions of suitably defined collective subspace. Such a microscopic description of the sub-barrier fusion permits the competing reaction mechanisms to be analyzed in a self-consistent and unified way. In a recent paper [28] it is found that the above-mentioned specific behavior of the mass parameter for the fusion reaction is originating from the pre-equilibrium nucleon exchange between colliding nuclei. The present paper considers further development and justification of the method [25–27]. In the next section we give a general outline of the problem and a hierarchy of approximations leading to the mean-field reduction of the many-body tunneling problem. In Sec. III we describe a numerical method for the solution of mean-field nuclear dynamics within the path integral framework in a subspace of collective variables and apply it for microscopic calculations of sub-barrier fusion cross sections. Our conclusions are presented in Sec. IV.

II. MEAN-FIELD APPROACH TO MANY-BODY TUNNELING

The complete microscopic description of a many-body system is provided by the N-body density matrix $\hat{\rho}_N$, which

*On leave from Institute for Nuclear Research, 47, Pr. Nauki, Kiev 262028, Ukraine.

satisfies the quantal Liouville equation of motion (cf., e.g., [21])

$$\frac{d\hat{\rho}_N}{dt}+i\hat{L}_N\hat{\rho}_N=0, \tag{1}$$

where $\hat{L}_N=\hbar^{-1}[\hat{H}_N,\cdot]$ is the quantal Liouville operator with the Hamiltonian $H_N=T+U_N[\{\mathbf{r}_i\}]$. Here T is the kinetic energy, and the N-body potential energy $U_N[\{\mathbf{r}_i\}]$ is determined by nucleon-nucleon interaction which is assumed to be local in time and configuration space. Equation (1) can be thought to describe a stochastic process of nuclear collision, where the N-body density matrix $\hat{\rho}_N$ is treated as a stochastic quantity fluctuating with respect to the collision events. An exact solution of Eq. (1) might generally provide a basis for an analysis of sub-barrier fusion. It is worth noticing, however, that to describe a process occurring with a probability of, say, 10^{-5} one has to generate more than 10^6–10^7 events, a number far beyond the most optimistic expectations of computer possibilities. It is, therefore, advantageous, e.g., to consider the average properties of a system with respect to the features of quantum tunneling. The mean-field reduction of a quantum many-body problem represents a useful framework for such a consideration. It is well known, indeed, that in the cases of low energetic nuclear scattering the Hartree mean-field approximation yields a realistic picture of the collision process. The effect of correlations at these conditions can be incorporated in a perturbative way using, e.g., a Boltzmann and/or Langevin (see, for example, [29] and references therein) type of approximation. Within such an approach the equation of motion for the many-body density matrix, Eq. (1), is reduced to the fluctuating one-body density matrix $\hat{\rho}$,

$$\frac{d\hat{\rho}}{dt}+i\hat{L}\hat{\rho}=I(\hat{\rho})+\delta K(t), \tag{2}$$

where $\hat{L}=\hbar^{-1}[h(\hat{\rho}),\cdot]$ denotes the one-body quantum Liouville operator corresponding to the self-consistent evolution of a system with a one-body Hamiltonian $h(\hat{\rho})=\hat{p}^2/2m+U[n]$, and the mean field $U[n]$ is related to a long-range part of the nuclear interaction and will be defined in next section [see Eq. (23)] through spatial nucleon density $n(\mathbf{r})=\langle\mathbf{r}|\hat{\rho}|\mathbf{r}\rangle$. The quantity $I(\hat{\rho})$ on the right-hand-side (RHS) of Eq. (2) corresponds, in general, to a memory-dependent binary collision term that simulates the short-range two-body nucleon-nucleon correlation effects during the evolution. The higher-order correlation effects are indicated in Eq. (2) by an additional term $\delta K(t)$ corresponding to a fluctuating part of the short-range correlations.

Some reaction channels of a nuclear collision can be identified and analyzed with the help of associated collective variables. For simplicity we consider here the fusion reaction in a head on collision of nearly symmetric pair of nuclei A and B. Then the associated collective variable $\hat{\mathcal{R}}=\Sigma_{k=1}^{A_{\rm tot}}\hat{R}_k$ and the collective momentum $\hat{\mathcal{P}}=\mu\Sigma_{k=1}^{A_{\rm tot}}\hat{P}_k$ can be naturally chosen to correspond to the Hermitian (see the Appendix) single-particle operators

$$\hat{R}=s(z-Z_0)(z-Z_0),\quad \hat{P}=\frac{1}{2}[\hat{p}_z s(z-Z_0)+s(z-Z_0)\hat{p}_z], \tag{3}$$

where the Z axis denotes the reaction axis,

$$s(x)=\begin{cases}-(A_{\rm A})^{-1} & \text{for } x<0,\quad A_{\rm A}=\int_{z<Z_0}d\mathbf{r}n(\mathbf{r}),\\ (A_{\rm B})^{-1} & \text{for } x>0,\quad A_{\rm B}=\int_{z>Z_0}d\mathbf{r}n(\mathbf{r}).\end{cases} \tag{4}$$

Here $A_{\rm A}$ and $A_{\rm B}$ give the mass numbers of ''each nucleus,'' the parameter Z_0 characterizes the position of a dividing plane and defines the mass asymmetry degree of freedom $\eta=(A_{\rm B}-A_{\rm A})/A_{\rm tot}$, $A_{\rm tot}=A_{\rm A}+A_{\rm B}$, along a fusion path, and the reduced mass $\mu=A_{\rm A}A_{\rm B}/A_{\rm tot}=(1-\eta^2)A_{\rm tot}/4$ is measured in units of the nucleon mass m. One can easily obtain (see the Appendix) the commutation relation $[\hat{\mathcal{R}},\hat{\mathcal{P}}]=i\hbar[1+O(\eta^2)]$ which suggests that the operators $\hat{\mathcal{R}}$ and $\hat{\mathcal{P}}$ are conjugate with an accuracy of η^2 and can be adopted for a case of nearly symmetric (e.g., $\eta<0.1$) configurations.

For the well-separated nuclei the expectation value

$$R=\langle\hat{\mathcal{R}}\rangle=Sp(\hat{R}\hat{\rho})=\int d\mathbf{r}s(z-Z_0)zn(\mathbf{r}) \tag{5}$$

gives the distance between the centers of mass of two colliding nuclei, while the expectation value

$$P=\langle\hat{\mathcal{P}}\rangle/\mu=\mathrm{Sp}(\hat{P}\hat{\rho}) \tag{6}$$

corresponds to the momentum of relative motion per nucleon. Everywhere below we refer for the value P as a collective momentum. The equations of motion for these expectation values provide a basis to study the fusion reaction channel. In the case of a nearly symmetric system we find that the mass asymmetry parameter plays a minor role since the related corrections in $\{R,P\}$ evolution are of order of η^2. Thus neglecting these terms it is straightforward to obtain for the collective coordinate

$$\dot{R}=\mathrm{Sp}(\hat{R}\dot{\hat{\rho}})=\hbar^{-1}\mathrm{Sp}(-i\hat{R}[H,\hat{\rho}])\approx\mathrm{Sp}(\hat{P}\hat{\rho})/m=P/m. \tag{7}$$

To derive an equation of motion for the expectation value of the collective momentum we note that the applications of a mean-field treatment to the studies of $\{R,P\}$ collective dynamics for intermediate-energy nuclear reactions, like quasifission, deep-inelastic scattering, and damped and dissipative collisions, have shown the importance of the nucleon exchange channel (for a review see [30]). When the system stays at the overlapping regime for a long time $\Delta\tau$ as compared to the nuclear response time $\tau_{\rm c}$ relevant for nucleon capture one is able to apply the ''randomization hypothesis'' and obtain the well-known ''window formula.'' This consid-

eration yields a realistic picture of the internal nuclear excitation and damping of the collective motion. An analysis of experimental data (cf. [30,31]) indicates that such a nuclear response time can be revealed to be $\tau_c \approx (1-2)\times 10^{-21}$ s. The theoretical estimates give up to an order of magnitude larger values for the nucleon capture time (cf. [32]).

It is the approaching stage of a nuclear collision at distances corresponding to the barrier top that determines the barrier penetration probabilities, the principal quantities characterizing nuclear fusion in the vicinity as well as below the barrier height. In particular, at sub-barrier energies the barrier penetrabilities are defined by the properties of a system in the classically forbidden region. The time scale corresponding to an evolution in this region (i.e., the imaginary time evolution; see discussion below) can be estimated in a general way through the barrier characteristic frequency (i.e., the curvature at the top ω) as $\Delta\tau \approx \omega^{-1}$. Since typically $\hbar\omega \approx 3-5$ MeV (cf. [28]), the related time interval $\Delta\tau \approx (1-2)\times 10^{-22}$ s is considerably smaller than the nuclear response time for nucleon capture. As is shown in Sec. III such an estimate is also supported by the results of microscopic calculations. Consequently, within this time scale the collision of initially spherical nuclei can be well described omitting the effects of correlations and fluctuations [i.e., RHS of Eq. (2)]. Then neglecting the nuclear response with respect to transferred nucleon capture we parametrize the one-body density matrix in a general form as

$$\langle \mathbf{r}|\hat{\rho}|\mathbf{r}'\rangle = \langle \mathbf{r}|\hat{\rho}_A|\mathbf{r}'\rangle \exp\{i(\mathbf{r}-\mathbf{r}')\mathbf{P}(1+\eta)/2\} + \langle \mathbf{r}|\hat{\rho}_B|\mathbf{r}'\rangle \exp\{-i(\mathbf{r}-\mathbf{r}')\mathbf{P}(1-\eta)/2\}, \quad (8)$$

with $\mathbf{P}=\{0,0,P\}$, $\hat{\rho}_A$ and $\hat{\rho}_B$ are generally distorted one-body density matrices of nuclei A and B with the centers of mass at rest. Using this parametrization we obtain the following equation of motion for the collective momentum:

$$\begin{aligned}\dot{P} &= 2^{-1}\mathrm{Sp}([s(z-Z_0)\hat{p}_z + \hat{p}_z s(z-Z_0)]\dot{\hat{\rho}}) \\ &= (2i\hbar)^{-1}\mathrm{Sp}([s(z-Z_0)\hat{p}_z + \hat{p}_z s(z-Z_0)]\cdot[\hat{h},\hat{\rho}]) \\ &= F \approx F^{\mathrm{l}} + F^{\mathrm{nl}},\end{aligned}$$

$$F^{\mathrm{l}} = \int d\mathbf{r}[-\partial_z U[n]\cdot n(\mathbf{r})s(z-Z_0) + \delta(z-Z_0)\Pi_{zz}(\mathbf{r})/(\mu m)],$$

$$F^{\mathrm{nl}} = \frac{P^2}{4\mu m}\int d\mathbf{r}\,\delta(z-Z_0)n(\mathbf{r}), \quad (9)$$

where $\Pi_{zz}(\mathbf{r}_0)=\mathrm{Sp}(\delta(\mathbf{r}-\mathbf{r}_0)\hat{p}_z^2\hat{\rho})$ denotes the diagonal component of the static [i.e., the c.m. system (c.m.s.) of A and B nuclei are at rest] pressure tensor. The first term on the RHS of Eq. (9) gives the local part (F^{l}) of the collective force, while the time-reversible nonlocal part (F^{nl}) of the collective force caused by the preequilibrium nucleon exchange is related to the distance dependent collective mass [14], since this part represents a bilinear form of the collective momentum P. In contrast to the ''randomization hypothesis'' approximation (i.e., zero nuclear response time), Eq. (9) does not contain the frictional force. This is a consequence of the time-reversible mean-field dynamics [21] given by Eq. (2) with omitted RHS terms. Note that a similar expression is also obtained within the semiclassical treatment based on the Vlasov transport equation [28]. As is pointed out above such a mean-field treatment can be thought to represent the average collision dynamics at energies well above and below the barrier top. In this sense Eqs. (7) and (9) have classical properties and are well suited to describe the various features of heavy-ion collisions in classically allowed domains of collective variables (see [20] and references therein). For example, in the case of a head-on collision we can calculate the potential barrier corresponding to the *static* interaction between two nuclei as

$$V_{\mathrm{int}}(R) = \left| \int_R^\infty dR\cdot F^{\mathrm{l}} \right|. \quad (10)$$

It is worth pointing out that within such a definition one takes into consideration the coupling of translational motion of nuclei to other degrees of freedom (e.g., nuclear deformation and polarization, neck formation) during the collision dynamics. This property gives rise to, e.g., the dependence of the interaction potential on the incident energy (see next section). In the following we will also consider the effective potential barrier

$$V_{\mathrm{eff}}(R) = \left| \int_R^\infty \mathrm{d}R\cdot F \right| \quad (11)$$

accounting for the nonlocal components of the collective force caused by the dynamical effect.

Equations (7) and (9) provide the basis for the description of the quantum effects related to the collective nuclear phenomena (e.g., fusion, fission) in the energy region below the Coulomb barrier. The quantum features with respect to the collective variables result in a finite value of the energy-dependent barrier penetration probability $T_l(E)$, at partial l wave for the beam energy E. Then the sub-barrier fusion cross section is written as [33,34]

$$\sigma(E) = \frac{\pi\hbar^2}{2\mu m E}\sum_{l=0}^{\infty}(2l+1)T_l(E). \quad (12)$$

Since for the nuclei of medium and large mass numbers many values of partial l waves contribute to the sum in Eq. (12), we can replace that sum by an integral. Furthermore, we assume that the l dependence of the transmission probability at a given energy can be approximated by simply shifting the energy [35,36]

$$T_l(E) \approx T_0\left(E - \frac{l(l+1)\hbar^2}{J_E}\right), \quad (13)$$

where $J_E = (A_{\mathrm{tot}} m\langle R^2\rangle_E)$ characterizes an effective moment of inertia, which is a slowly varying function of the energy E [28,37,38], $\langle R^2\rangle_E = \langle(\mathbf{r}-\mathbf{R}_{\mathrm{c.m.}})^2\rangle_{t_2}$, t_2 is the time when the

distance between the centers of mass of two nuclei has the value of barrier top position, and $\mathbf{R}_{\text{c.m.}} \equiv \langle \mathbf{r} \rangle_{t_2}$ is the position of the center of mass of a dinuclear system. Then we calculate the total cross section according to [36] as

$$\sigma(E) \approx \pi \frac{J_E}{\mu E} \int_{-\infty}^{E} dE' T_0(E'). \tag{14}$$

To obtain the penetration probability at the energies above the Coulomb barrier we use the Hill-Wheller formula (cf. [34])

$$T_0(E) = (1 + \exp\{-\pi \mu P_{t_2} v_{t_2} / 2\hbar\omega\})^{-1}, \tag{15}$$

where P_{t_2} and v_{t_2} refer to the collective momentum and the velocity $v = dR/dt$ for the dynamics in the $\mathbf{R}$ direction (e.g., the beam axis) calculated at time step t_2 (see above).

In the energy region below the barrier we employ the Feynman path-integration technique within the microscopic treatment. For a given path connecting the entrance and exit channels of a fusion reaction the probability for a sub-barrier process is obtained from the equations

$$T_0(E) = (1 + \exp\{2\mu S/\hbar\})^{-1}, \quad S = \int |P^{\text{I}}| \mathrm{d}R^{\text{I}}, \tag{16}$$

where the action S corresponds to the self-consistent evolution along a path in classically forbidden region and is determined by the respective collective coordinate $\mathbf{R}^{\text{I}}$ and momentum $\mathbf{P}^{\text{I}}$.

The classically forbidden region for the collective variables becomes accessible after the so-called Wick transformation, $t \to i\tau$, where τ is real. Changing simultaneously $P \to -iP^{\text{I}}$ in Eqs. (7) and (9) we get the following equation of motion for $\{\mathbf{R}^{\text{I}}, \mathbf{P}^{\text{I}}\}$ imaginary time evolution:

$$\frac{d\mathbf{R}^{\text{I}}}{d\tau} = \frac{\mathbf{P}^{\text{I}}}{m}, \quad \frac{d\mathbf{P}^{\text{I}}}{d\tau} = \mathbf{F}^{\text{I}} \approx -\mathbf{F}^{\text{l}} + \mathbf{F}^{\text{nl}}. \tag{17}$$

From these equations we see that the path leading to a sub-barrier fusion is associated with the dynamics in an inverted potential barrier [i.e., the negative sign of the local collective force; see Eq. (10)], while the nonlocal component remains unchanged. This feature of a fusion path can be also obtained going through the standard steps of WKB approximation applied to the collective degrees of freedom when accounting for the variation of the respective inertia parameter [14]. Such a property results in the lower and thinner effective barrier for the imaginary time propagation [i.e., $V^{\text{I}}_{\text{eff}}$ given by Eq. (11) with the collective force $\mathbf{F} = -\mathbf{F}^{\text{I}}$ from Eq. (17)] as compared to the associated potential barrier and therefore in an enhancement of the fusion cross section [28].

It is worth noticing that the fluctuation effects are expected to give rise to an additional enhancement of the penetration probability at sub-barrier energies. For instance, assuming small Gaussian fluctuations of action (δS) around its average value the enhancement factor can be estimated to give $F_{\text{enh}} \approx \exp\{\mu^2 \overline{\delta S^2}/\hbar^2\}$, where an overbar denotes an ensemble averaging with respect to the collision events. Thus in some cases, like nonspherical nuclei [39], the action fluctuations may enhance considerably the fusion cross section as compared to the average description.

III. PATH INTEGRALS VERSUS MICROSCOPIC EVOLUTION

A. Imaginary time kinetics

In the samples of calculations below we further simplify the nuclear many-body problem by employing a semiclassical treatment for intrinsic degrees of freedom. Within this treatment, the principal quantity is the Wigner phase-space distribution function $f(\mathbf{r},\mathbf{p};t)$ which is related to the one-body density matrix through the Wigner transform [21,40]

$$f(\mathbf{r},\mathbf{p};t) = (2\pi\hbar)^{-3} \int d\mathbf{q}\, d\mathbf{q}_1 \exp[-i(\mathbf{q}-\mathbf{q}_1)\mathbf{p}/\hbar] \times \langle \mathbf{q}|\hat{\rho}(t)|\mathbf{q}_1\rangle \delta\left(\mathbf{r} - \frac{\mathbf{q}+\mathbf{q}_1}{2}\right). \tag{18}$$

The expectation value of an observable $\hat{A}(\hat{\mathbf{r}},\hat{\mathbf{p}})$ is represented as

$$\langle A \rangle = \int d\mathbf{r}\, d\mathbf{p} A(\mathbf{r},\mathbf{p}) f(\mathbf{r},\mathbf{p};t). \tag{19}$$

In the Wigner representation the quantum mean-field Liouville equation [i.e., Eq. (2) with the RHS put to zero] is given by

$$\frac{\partial f}{\partial t} = -\hat{L}_{\text{W}} f, \tag{20}$$

where the quantum Liouville operator $\hat{L}_{\text{W}}$ has the form

$$\hat{L}_{\text{W}} = \hat{L}_0 + \hat{L}_{\text{q}}, \quad \hat{L}_0 = \frac{\mathbf{p}}{m} \vec{\partial}_{\mathbf{r}}, \tag{21}$$

$$\begin{aligned} \hat{L}_{\text{q}} f &= \int \frac{d\mathbf{q}d\mathbf{p}_1}{\hbar(2\pi\hbar)^3} \sin\left(\frac{(\mathbf{p}-\mathbf{p}_1)\mathbf{q}}{\hbar}\right) [U(\mathbf{r}-\mathbf{q}/2) \\ &\quad - U(\mathbf{r}+\mathbf{q}/2)] f(\mathbf{q},\mathbf{p}_1;t) \\ &= -\sum_{n=0}^{\infty} \frac{(-1)^n}{(2n+1)!} \left(\frac{\hbar}{2}\right)^{2n} U[n] (\vec{\partial}_{\mathbf{r}} \vec{\partial}_{\mathbf{p}})^{2n+1} f. \end{aligned} \tag{22}$$

We use the following parametrization of the time-dependent mean field $U[n]$ in our calculations:

$$\begin{aligned} U[n] &= a\left(\frac{n(r)}{n_0}\right) + b\left(\frac{n(r)}{n_0}\right)^{\gamma} + c\tau_3(n_{\text{n}} - n_{\text{p}}) \\ &\quad + \int d\mathbf{r}_1 \left(V_\pi r_\pi \frac{\exp\{-|\mathbf{r}-\mathbf{r}_1|/r_\pi\}}{|\mathbf{r}-\mathbf{r}_1|} n(\mathbf{r}_1) \right. \\ &\quad \left. + \frac{e^2}{|\mathbf{r}-\mathbf{r}_1|} n_{\text{p}}(\mathbf{r}_1) \right), \end{aligned} \tag{23}$$

where n_n, n_p, and n are the neutron, proton, and total nuclear density; $n_0 \approx 0.15$ fm^{-3}; $r_\pi = \hbar/m_\pi c \approx 1.4$ fm and τ_3 is the isospin projection operator. The set of parameters for the nucleon-nucleon interaction corresponds to the compressibility $K = 200$ MeV of an infinite nuclear matter at normal density, i.e., $\tilde{a} = a + 4\pi n_0 r_\pi^3 V_\pi = -356$ MeV, $b = 303$ MeV, and $\gamma = 7/6$, and the constant relevant for the symmetry potential $c = 32$ MeV/n_0. The value $V_\pi \approx -6.43$ MeV is chosen in order to reproduce (see below and Ref. [27]) the (^{16}O+^{16}O) fusion barrier derived from the fusion data [36]. We note that this value is consistent with the contribution of *one-pion* exchange to the nucleon-nucleon interaction [41]. In many cases of a many-body problem (e.g. systems at high entropy) one can assume convergence of the series in Eq. (22) [42,43] and consider quantum correction terms as a perturbation to the classical motion, which is governed by the gradient part of the quantum Liouville operator given by Eq. (22). Thus the quantal effects can be included in a perturbative way by using, e.g., the quantum test particle (QTP) method [23]. This method has been applied [24] to a description of various type perturbative quantum effects in a semiclassical nuclear mean-field dynamics, like nucleon tunneling phenomena, coherence effects, etc. In this paper we focus on the semiclassical feature and neglect the quantum perturbation with respect to the internal motion.

The collective quantum phenomena in certain collective subspace, on the other hand, can be treated by making use of the Feynman path-integral technique [i.e., Eq. (17)]. The Wick transformation can be incorporated into the mean-field transport equations replacing the one-body Liouville operator by

$$\text{(i)} \quad \hat{L} \to \hat{L}^{\mathrm{I}} = \hat{L} + i\hbar^{-1} \cdot [2F^{\mathrm{I}}(z - Z_0) s_{\mathrm{I}}(z - Z_0), \cdot] \quad (24)$$

in the TDHF formulation or

$$\text{(ii)} \quad \hat{L}_{\mathrm{W}} \to \hat{L}^{\mathrm{I}}_{\mathrm{W}} = \hat{L}_{\mathrm{W}} + i \cdot 2F^{\mathrm{I}} s_{\mathrm{I}}(z - Z_0) \cdot \partial_{p_z} \quad (25)$$

in the Wigner formulation. Here the form

$$s_{\mathrm{I}}(x) = \begin{cases} -A_{\mathrm{B}}/A_{\mathrm{tot}} & \text{for } x < 0, \\ A_{\mathrm{A}}/A_{\mathrm{tot}} & \text{for } x > 0, \end{cases}$$

ensues, by a consistency with Eq. (17) and the condition of zero force acting on the c.m. of a system, i.e., vanishing averaged value of an additional term in Eqs. (24) and (25).

B. Numerical method

A straightforward way to realize the semiclassical concept presented above is provided by using the test-particle (TP) ansatz [21–24], where one considers the phase-space Wigner distribution function $f(\mathbf{r},\mathbf{p};t)$ [see Eq. (18)] as a collection of the phase-space cells $|\Gamma_i\rangle\rangle$ (TP), which behave like classical particles,

TABLE I. Binding energies per nucleon (MeV) and root mean square radii (fm).

	^{16}O	^{40}Ca	^{58}Ni	^{90}Zr	^{208}Pb
E/A expt.	-7.98	-8.55	-8.73	-8.71	-7.87
Vlasov	-8.8	-8.77	-9.18	-9.00	-8.23
rms expt.	2.73	3.49	3.82	4.27	5.5
Vlasov	2.75	3.50	3.99	4.50	5.75

$$f(\mathbf{r},\mathbf{p};t) = \frac{1}{N}\sum_{i=1}^{M} |\Gamma_i\rangle\rangle, \quad |\Gamma_i\rangle\rangle \equiv \delta(\mathbf{r} - \mathbf{r}_i(t))\,\delta(\mathbf{p} - \mathbf{p}_i(t)), \quad (26)$$

$$\delta\mathbf{r}_i = \delta t\, \mathbf{p}_i/m, \quad \delta\mathbf{p}_i = -\delta t\, \boldsymbol{\partial}_{\mathbf{r}} U(\mathbf{r}_i),$$

$$i = 1, \ldots, M = N(A_{\mathrm{A}} + A_{\mathrm{B}}), \quad (27)$$

where N is an integer large enough to ensure numerical convergency and is associated with a number of TPs per nucleon.

As the initial conditions we distribute the TPs of the colliding nuclei in configuration space according to the Thomas-Fermi density associated with the Woods-Saxon potential: $\rho(r) \sim [E_{\mathrm{F}} - U_{\mathrm{WS}}(r)]^{3/2}$. The self-consistent mean field [i.e., Eq. (23)] is determined in each cube of the size 1 fm^3 in configuration space. The TP distribution in momentum space is given by the Thomas-Fermi relation regarding the respective mean field. Approximately stationary solutions of the Vlasov equation are found with the parameters of the Woods-Saxon potential given in [22] (for more details see also, e.g., [23,24]). From Table I we see that the present procedure reproduces the experimental results for the binding energies and the root mean square (rms) radii of spherical nuclei within the same quality as other methods (cf. [21,22] and references therein). We would like to remark that the application of the TP method requires an accurate stability of the solution especially with respect to the energy conservation when propagating in time with Eqs. (26) and (27). Such a requirement can be achieved by using relatively small time steps and a large number of TPs (see, for example, the analysis given in Refs. [24,44]). In our experience we find that for nuclei of medium mass numbers the proper accuracy of energy conservation (to better than 1% from the value of potential barrier height with respect to the collective degrees of freedom [45]) is obtained at, e.g., the total number of TPs of 10^5 and varied time steps: $\delta t \approx 0.2$ fm/c at relatively large distances when the Coulomb contribution to the potential barrier [i.e., Eq. (10)] is dominant, and $\delta t \approx 0.05$ fm/c at small distances where the nuclear part plays a major role.

By using the TP method it is simple to specify further the equation of motion for the collective degrees of freedom. Inserting Eq. (26) into Eq. (19) for expectation values R and P we write the collective coordinate and momentum as

$$\begin{Bmatrix} \mathbf{R} \\ \mathbf{P} \end{Bmatrix} = N_{\mathrm{A}}^{-1} \sum_i^{N_{\mathrm{A}}} \begin{Bmatrix} \mathbf{r}_i \\ \mathbf{p}_i \end{Bmatrix} - N_{\mathrm{B}}^{-1} \sum_i^{N_{\mathrm{B}}} \begin{Bmatrix} \mathbf{r}_i \\ \mathbf{p}_i \end{Bmatrix}. \quad (28)$$

Here and below the indices A and B indicate that the respective sums are taken over the total number N_A and N_B of TPs belonging to the nuclei A and B, respectively. The variation of this relation at small time interval δt reads

$$\begin{Bmatrix} \delta\mathbf{R} \\ \delta\mathbf{P} \end{Bmatrix} = \frac{\delta t}{N_A} \sum_i^{N_A} \begin{Bmatrix} \mathbf{p}_i/m \\ -\boldsymbol{\partial}_\mathbf{r} U(\mathbf{r}_i) \end{Bmatrix} - \frac{\delta t}{N_B} \sum_i^{N_B} \begin{Bmatrix} \mathbf{p}_i/m \\ -\boldsymbol{\partial}_\mathbf{r} U(\mathbf{r}_i) \end{Bmatrix} - \frac{N_A+N_B}{N_A N_B} \left(\sum_i^{\delta N_{A\to B}} \begin{Bmatrix} 0 \\ \mathbf{p}_i \end{Bmatrix} - \sum_i^{\delta N_{B\to A}} \begin{Bmatrix} 0 \\ \mathbf{p}_i \end{Bmatrix} \right), \quad (29)$$

where the sum in the third term of the RHS of this equation is running over the TPs which are transferred from nucleus A to nucleus B ($\delta N_{A\to B}$) and from B to A ($\delta N_{B\to A}$), respectively. This term arises due to the nucleon exchange through the neck region.

The local part of the collective force $\mathbf{F}^{\mathrm{l}}$ can be calculated according to the relation

$$\mathbf{F}^{\mathrm{l}} \approx \frac{1}{N} \sum_i^M [-\boldsymbol{\partial}_\mathbf{r} U(\mathbf{r}_i)] s(z_i - Z_0) + \mathbf{n}_z \frac{\Pi_0}{\mu} \times \int d\mathbf{r}\, \delta(z - Z_0) [n(\mathbf{r})]^{5/3}, \quad (30)$$

where the constant $\Pi_0 = (3\pi^2/2)^{2/3}\hbar^2/5m \approx 50$ MeV fm^2 corresponds to the static pressure tensor of the Fermi liquid at zero temperature, and $\mathbf{n}_z$ denotes a unity vector indicating the Z direction. On the basis of this equation we choose the position of a dividing plane Z_0 in order to minimize the potential barrier, Eq. (10), along the fusion path. This condition corresponds to the minima of the second term on the RHS of Eq. (30). We note that for the cases considered below the mass asymmetry parameter η remains small during the evolution.

It is straightforward now to apply the Feynman method in order to find in a self-consistent manner the path for a channel of sub-barrier fusion reaction. We simulate the semiclassical imaginary time evolution in collective subspace $\{\mathbf{R},\mathbf{P}\}$ [i.e., the Wick transformation; see Eqs. (17) and (25)] replacing the equations of motion, Eq. (27), by

$$\delta\mathbf{r}_i^{\mathrm{I}} = \delta t\, \mathbf{p}_i^{\mathrm{I}}/m, \quad \delta\mathbf{p}_i^{\mathrm{I}} = -\delta t(\boldsymbol{\partial}_\mathbf{r} U(\mathbf{r}_i^{\mathrm{I}}) + 2\mathbf{F}^{\mathrm{l}} s_{\mathrm{I}}(z_i^{\mathrm{I}} - Z_0)), \quad (31)$$

where $\mathbf{p}_i^{\mathrm{I}}$ and $\mathbf{r}_i^{\mathrm{I}}$ denote the imaginary time coordinate and momentum of ith TP. We would like to stress that within such a description also other collective degrees of freedom remain unfrozen along the fusion path. This feature is preserved due to a self-consistent treatment employed for the evolution in classically forbidden region. It should be noted, however, that some specific cases may require in general an explicit consideration of the tunneling in a direction of some additional collective degrees of freedom other than **R** and **P** (cf. [14]), for instance, the neck region and mass asymmetry. The previous studies (cf. [20,21]) have shown, indeed, that the collective degrees of freedom **R** and **P** adopted here are sufficient to describe the fusion dynamics above the barrier especially for light and medium nearly symmetric systems. It can be expected that similar properties hold at the energies near the Coulomb barrier [10,33,36,39,46]. For heavier systems this might not be the case and one possibly needs to introduce additional degrees of freedom as an explicit tunneling variable.

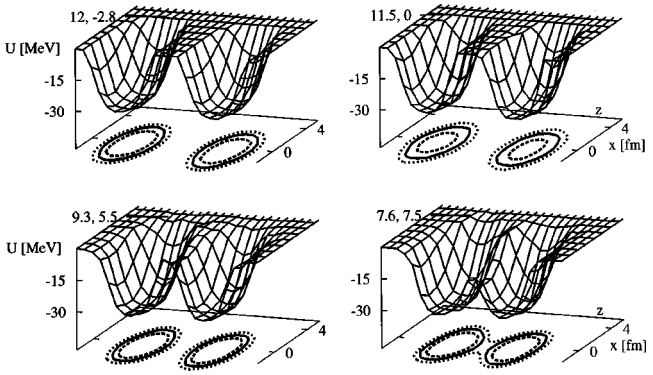

FIG. 1. Snapshots from the mean-field simulation of the fusion reaction for a head-on ^{16}O+^{16}O collision at the energy 8 MeV. The surfaces represent the neutron mean field. The contours in the XZ plane show the neutron density at 0.015 fm^{-3} (dotted lines), 0.03 fm^{-3} (solid lines), and 0.05 fm^{-3} (dashed lines). The numbers indicate the relative distance (the first number measured in fm) between the c.m.s. of two nuclei and the time (the second number measured in 10^{-22} s) during the evolution along the fusion path. $t=0$ corresponds to the outer turning point.

C. Deformation, neck, and nonlocality in nuclear fusion energetics

The snapshots from the sample of calculations for ^{16}O $+^{16}$O sub-barrier fusion reaction are given in Fig. 1. The relative distances between 11.5 and 7.6 fm represent the classically forbidden domain. To access these distances we make use of the method discussed above for a sub-barrier collision. We switch on the imaginary time propagation with respect to the collective subspace [see Eqs. (17), (25), and (31)] at the outer classical turning point ($R \approx 11.5$ fm), where the nuclei stop because the relative motion in the R direction is slowed down by Coulomb repulsion. The contribution of the Coulomb interaction to the collective force is turned on to be attractive after this time step and the centers of mass of the nuclei are accelerated towards each other until the nuclear forces start to grow in importance. Since along the fusion path in the classically forbidden domain the nuclear forces contribute repulsively to the collective force with respect to the motion in the R direction, the nuclei stop again at the inner classical turning point ($R \approx 7.6$ fm). Switching from the imaginary time evolution to the real one at this point, it is possible to analyze the dynamics and the properties of the evaporative residue. In Fig. 1 one sees that during the evolution in classically forbidden region (i.e., the imaginary time evolution) light nuclei overlap negligibly even in the vicinity of inner turning point, displaying thereby an applicability of models based on the picture of nuclear proximity energy (cf. [47,48]). Within such a picture the fusion barrier is given as contributions of the Coulomb repulsion and the attractive nuclear interaction between the

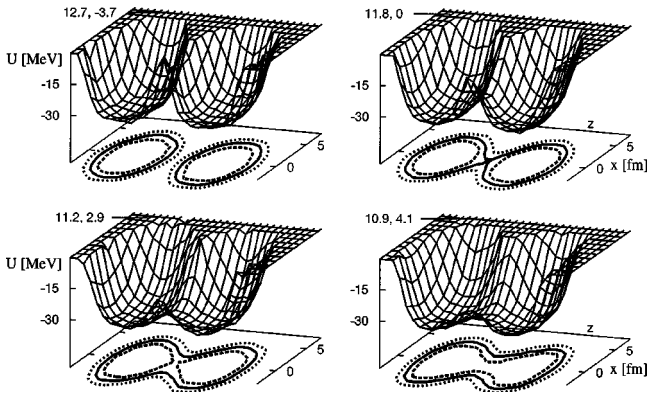

FIG. 2. The same as Fig. 1 for a ^{58}Ni+^{58}Ni collision at the energy 93 MeV.

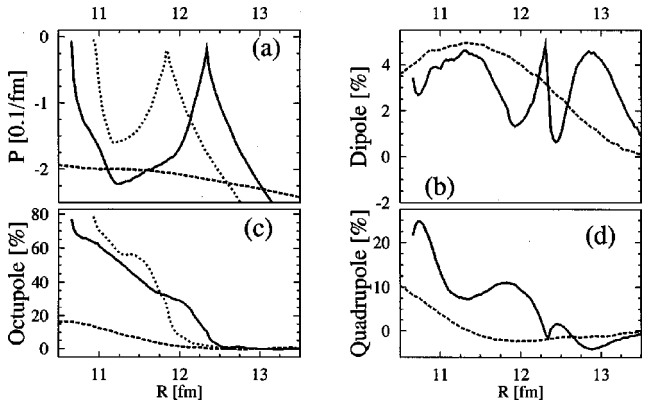

FIG. 3. The phase-space diagram [(a) upper part of the left panel] for the collective variables $\{R,P\}$ and the values β_l [$l=1$, (b) upper part of the right panel; $l=2$, (d) bottom part of the right panel; and $l=3$, (c) bottom part of the left panel] corresponding to a head-on ^{58}Ni+^{58}Ni collision at the beam energies 90 MeV (solid line), 93 MeV (dotted line), and 145 MeV (dashed line). In the cases of 90 MeV and 93 MeV plotted is the collective momentum P that is multiplied by a factor of 3.

nuclear surfaces which is related to the long-range component of nuclear forces. Since the effects of nuclear polarization and deformation as well as nonlocality in sub-barrier fusion of a light system are small, the long-range component of the nuclear interaction can be revealed from the fusion data (see Fig. 4 and discussion therein).

In Fig. 2 we show the snapshots from the simulations for the sub-barrier fusion of (^{58}Ni+^{58}Ni) system. In contrast to a light system, for such nuclei of medium mass numbers the formation of a neck can be considered as the predominant mechanism leading to the creation of a united residue during the imaginary time evolution.

As it is seen in Figs. 1 and 2 for nuclei of relatively small and medium mass numbers the obtained time interval $\Delta\tau$ corresponding to the noticeable nucleon exchange (i.e., pronounced nuclear density in the neck region) is in good agreement with an estimate based on the barrier curvature parameter (see Sec. II).

To analyze the role of nuclear deformation in the nuclear fusion process we consider the behavior of multipole moments of colliding nuclei using the quantities

$$\beta_l=(2l+1)\frac{\langle r^l\cdot P_l(\hat{\mathbf{r}})\rangle_{\mathrm{A}}+(-1)^l\langle r^l\cdot P_l(\hat{\mathbf{r}})\rangle_{\mathrm{B}}}{\langle r^l\rangle_{\mathrm{A}}+\langle r^l\rangle_{\mathrm{B}}} \qquad (32)$$

for quadrupole ($l=2$) and octupole ($l=3$) components. Here P_l are the Legendre polynomials, and $\langle\cdot\rangle_{\mathrm{A}}$ and $\langle\cdot\rangle_{\mathrm{B}}$ denote an average with respect to the nuclei A and B. The dipole moment is characterized by the normalized proton polarization distance, i.e., the quantity

$$\beta_1=3\frac{R_{\mathrm{p}}-R}{\langle r\rangle_{\mathrm{A}}+\langle r\rangle_{\mathrm{B}}}, \qquad (33)$$

where R_{p} is the distance between the centers of masses of the protons belonging to the nuclei A and B, respectively.

The quantities β_l are shown in Fig. 3 together with the $\{R,P\}$ phase-space diagrams. One sees that at beam energies well above the Coulomb barrier only a high-frequency dipole component of the nuclear deformation has sufficient time to be excited. The excitation amplitude of this component is, however, rather small because of the large stiffness of the dipole mode. The low-frequency octupole degree of freedom [see Fig. 3(c)] is released to a large amplitude especially at energies near to the barrier. Since the translational motion of nuclei is very slow in such a case, this degree of freedom has sufficient time to be excited. The progressive growth of octupole deformation along the fusion path is related to the creation of the nuclear density in the neck region and the nucleon exchange. This mechanism leads to the formation of an intermediate dinuclear system during the fusion reaction (see also Fig. 2). This stage of the evolution proceeds until the inner turning point and thereafter before the two nuclei actually fuse. The intermediate-frequency quadrupole deformation component [see Fig. 3(d)] shows a change in the nuclear shape at the approaching stage from an oblate configuration at relatively large distances where the repulsive Coulomb interaction is dominant to a prolate shape at smaller R when the attractive nuclear interaction becomes noticeable. This feature is also shown by the results of calculations [47] based on the liquid drop model. However, the dynamical effects smear out a sharp change in the nuclear shape transition. The quadrupole deformation displays pronounced oscillations at sub-barrier energies, resulting thereby in an oscillating behavior of the neck size.

As is pointed out above the long-range component of the nuclear interaction can be extracted from the data on sub-barrier fusion of light spherical nuclei. Within the parametrization given by Eq. (23) this component is determined by the strength of a long-range one-pion exchange contribution to the nucleon-nucleon interaction [41]. Figure 4(a) shows the potential barriers evaluated according to Eq. (10) for a head-on (^{16}O+^{16}O) collision at the fixed value $V_\pi=-6.43$ MeV in Eq. (23). The cases of an incident energy below and well above the barrier are displayed to yield very similar interaction barriers, being in a good agreement with the one extracted from experimental data [36]. For nuclei of medium mass numbers the dependence of an amplitude of the nuclear deformation on the beam energy gives rise to a

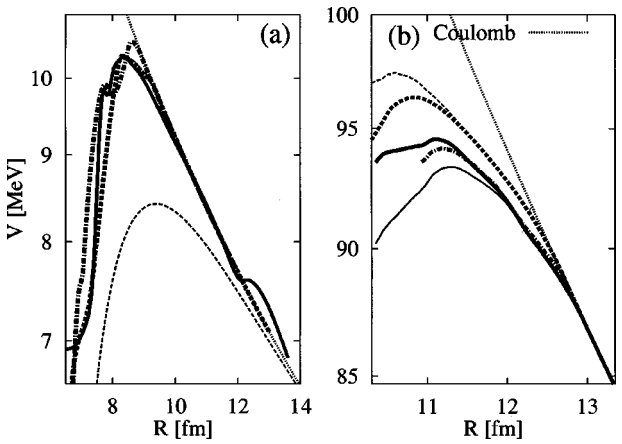

FIG. 4. The potentials for the fusion reaction. (a) Left panel represents $^{16}O+^{16}O$ system: the solid line shows the empirical potential [36], the dashed and dash-dotted lines are the results of the Vlasov simulations at the energies 8 MeV and 16 MeV, respectively, and the thin dashed line denotes the Bass parametrization [49]. (b) Right panel shows the results of the Vlasov simulations for a $^{58}Ni+^{58}Ni$ reaction at the energies 90 MeV (solid line), 93 MeV (dash-dotted line), and 145 MeV (dashed line). The thick lines indicate the potential barriers, while the thin lines represent the effective barriers. The thin dotted lines give the values of the Coulomb interaction between the pointlike charges.

variation of the potential barrier with the incident energy. It is a general feature of the nuclear collision that the neck formation results in a lowering of the potential barrier (cf. [50]). As is seen from Fig. 4(b) such a barrier lowering is the most significant at beam energies near to the barrier height. Since at this condition the deformation degrees of freedom are released at an early stage of the collision (see Fig. 3), the process of neck formation occurs at larger relative distances as compared to an overbarrier collision. This feature of the excitation of the collective degrees of freedom in nuclear tunneling contributes to an enhancement of the fusion cross section and can be thought to represent the semiclassical counterpart of the coupled-channel treatment (cf. [5,7]).

We finally discuss the effects of nonlocality in nuclear fusion energetics. As is demonstrated in Sec. II within the mean-field transport theory these effects can be understood in terms of the preequilibrium nucleon exchange through the neck region. In the cases of overbarrier energies such an effect gives rise to a larger value of the effective barrier, Eq. (11), as compared to the potential barrier [see Fig. 4(b)], representing thereby a feature similar to an ''extrapush effect'' (cf. [48] and references therein). When the beam energy is very close to the potential barrier height the collective momentum P approaches zero at the distances corresponding to the barrier top. As a consequence, the nonlocal component of collective force [see Eq. (9)] and, respectively, the difference between effective and potential barriers almost vanish at these energies. For instance, for a $^{58}Ni+^{58}Ni$ collision at the energy 93 MeV the potential and effective barriers [i.e., dash-dotted line in Fig. 4(b)] practically coincide. For a sub-barrier fusion process the nonlocal effects make the effective barrier thinner and lower than the potential one. Furthermore, since the neck appears at an early stage for the sub-barrier collision, the nonlocal effects are more important as compared to the overbarrier scattering. With decreasing the collision energy below the barrier the effects of nonlocality in the nucleus-nucleus interaction become more pronounced, yielding an additional enhancement of the fusion cross section, a property which is generally not included explicitly within a coupled-channel treatment.

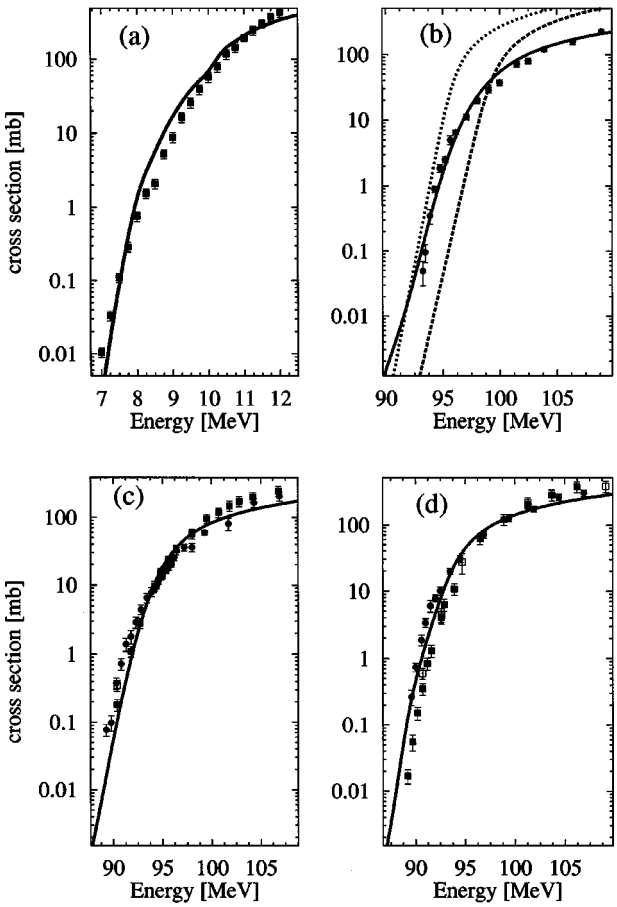

FIG. 5. The fusion excitation functions. Part (a) represents the $^{16}O+^{16}O$ system with the experimental data from Ref. [47]. Parts (b)–(d) display the results for the isotope pairs: (b) $^{58}Ni+^{58}Ni$; (c) $^{58}Ni+^{64}Ni$; and (d) $^{64}Ni+^{64}Ni$. The circles show the experimental results of Refs. [10,51] while the squares are taken from Ref. [52]. The solid lines denote the results of the Vlasov simulations; the dotted and dashed lines are obtained with the WKB approximation using the potential barriers of Fig. 4(b) corresponding to the beam energies 90 MeV (dotted curve) and 145 MeV (dashed curve).

D. Nuclear fusion cross section: The scaling properties

The total fusion cross section versus the beam energy is given in Fig. 5. As we have seen above the maximum of the interaction barrier between relatively light nuclei is located at large relative distance [see Figs. 1 and 4(a)]. Therefore, the nonlocal component of the collective force does not give any noticeable contribution. Consequently, a simple barrier penetration model based on the WKB approximation provides a realistic picture of the sub-barrier fusion for such a system. The height of the potential barrier in this case is determined by competition between the nuclear surface term

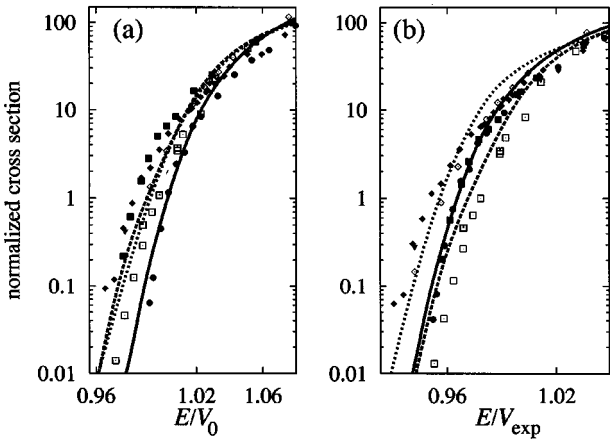

FIG. 6. The normalized fusion excitation functions for the isotope pairs ^{58}Ni+^{58}Ni (solid lines; the circles are the data from Refs. [10,51]), ^{58}Ni+^{64}Ni (dotted lines; the solid diamonds are the data from Refs. [10,51]; the open diamonds and triangles are the data from Ref. [52]), and ^{64}Ni+^{64}Ni (dashed line; the solid squares are the data from Refs. [10,51]; the open squares are the data from Ref. [52]). The fusion cross sections are scaled using the empirical values (V_{expt}, R_{expt}) given in Ref. [10] [(b), right panel], and the barrier heights V_0 and the value $\langle R^2 \rangle$ extracted from the numerical simulations at near to the barrier energies [(a), left panel]. The scaled cross sections are multiplied by the factors 0.5×10^3 (a) and 10^3 (b) for simplicity of presentation.

and the Coulomb interaction. The present parametrization of the nuclear interaction yields rather good agreement of the calculated cross section and the experimental data shown in Fig. 5(a). Some discrepancy at low energies is associated with the rough approximation of the continuously changing angular momentum made in Eq. (14) because the dependence of the transmission coefficient on angular momentum is relatively sharp for the case of light nuclei.

For heavier nuclei the effects of deformation, neck formation, and nonlocality grow in importance affecting considerably the fusion cross section [28]. From Fig. 5(b) we see that the experimentally observed sub-barrier enhancement can be understood as a barrier lowering property caused by polarization and deformation effects. At beam energies above the barrier height the fusion cross section obtained in the Vlasov simulations is systematically lower than the simple WKB barrier penetration prediction. Such a suppression is due to the nonlocality giving rise to the higher effective barrier as compared to the potential barrier [see Fig. 4(b)]. On the contrary, the effective barrier is suppressed at the sub-barrier energies. Consequently, in this energy range the fusion cross section is enhanced due to the nonlocal effects which become more pronounced with decreasing collision energy. As it is seen in Figs. 5(b)–5(d) such a property of nonlocality regarding the nonadiabatic features of the dynamics in classically forbidden region is essential for a good fit to data.

An analysis of the scaling properties of the cross section (see Fig. 6) for the various isotope pairs allows one to obtain further information regarding the mechanisms of the fusion excitation function enhancement. Such an analysis has been already employed, e.g., in Refs. [4,6,10,52] where the scaling has been discussed with respect to fixed energy-independent barrier height. The barrier has been obtained from a fit to experimental data. Presented in Fig. 6(b) is such a scaling which displays an enhancement for an asymmetric system when only one of the colliding nuclei contains extra neutrons. In the Ref. [52] this property has been attributed to the coupling of the translational motion to $2n$ exchange channel. Figure 6(a) presents the results using the barrier heights obtained from the simulations at collision energy near to the barrier top. This scaling indicates that an enhancement in the fusion excitation function can be considered as a general feature for the neutron-rich system. These properties seem to point out that nonadiabatic effects related to preequilibrium nucleon flux in the neck region play a significant role in such an enhancement of the cross section.

IV. CONCLUSION

We have discussed a unified treatment for the microscopic description of nuclear fusion phenomena at the beam energies above as well as below the Coulomb barrier. Within the framework of this approach the fusion problem is treated by using the self-consistent mean-field evolution of a system and including the channel of the sub-barrier fusion reaction as a semiclassical propagation in the classically forbidden region of a collective subspace. Since the time interval of the evolution in the classically forbidden domain is shown to be an order of magnitude less than the nuclear response time with respect to the nucleon capture, the treatment of the time-reversible nuclear dynamics is justified within this time scale. The preequilibrium nucleon exchange through the neck region at an approaching stage of the nuclear collision is found to give rise to the nonlocality of the nucleus-nucleus interaction. These nonlocal effects can be considered in terms of an effective mass for the translational motion, which shows a decrease with decreasing relative distance.

The microscopic simulations indicate that the simple barrier penetration model yields realistic picture of nuclear fusion for light spherical nuclei. Therefore, the fusion data provide information regarding the barrier properties. This information allows one to obtain the surface component of a nucleus-nucleus interaction, which we describe in terms of a long-range one-pion exchange contribution to the nucleon-nucleon interaction. The strength of this contribution is extracted to be $V_\pi \approx -6.43$ MeV, in good agreement with an estimate of Ref. [41].

For heavier nuclei of medium mass numbers the effects of nuclear deformation, neck formation, and nucleon exchange grow in importance, modifying thereby the results of the WKB approximation considerably. We have seen that nuclear deformation and neck formation give rise to a beam energy dependence of the potential barrier. As is displayed in Fig. 4 such a barrier variation shows the same order of magnitude as respective barrier fluctuations obtained within a coupled-channel model, thus representing a semiclassical picture of the coupled-channel property. This feature can be regarded as a predominant mechanism of the nuclear fusion cross section enhancement at energies in the vicinity of the barrier top.

An analysis of the scaling properties in the fusion cross

section for different isotope pairs indicates that the fusion excitation function for nuclei containing extra neutrons displays in the low-energy region an enhancement as compared to the neutron-poor system. This enhancement can be attributed to nonadiabatic effects in the collective motion due to the preequilibrium nucleon exchange through the neck region.

ACKNOWLEDGMENTS

We want to thank Prof. N. Takigawa for valuable discussions as well as Prof. G. Royer for useful comments and interesting suggestions. The hospitality of the research group for Hadron Science, JAERI, as well as financial support from the Japan STA program are gratefully acknowledged by one of us (V.N.K.).

APPENDIX: UNCERTAINTY COMMUTATION RELATION FOR OPERATORS $\hat{\mathcal{R}}$ AND $\hat{\mathcal{P}}$

To calculate the commutator $[\hat{\mathcal{R}},\hat{\mathcal{P}}]$ we represent the function $s(x)$ defined by Eq. (4) as

$$s(x)=[\mathrm{erf}(a\cdot x)|_{a\to\infty}-\eta]/(2\mu), \tag{A1}$$

with the error function $\mathrm{erf}(x)=(2/\sqrt{\pi})\int_0^x \exp\{-u^2\}du$. Since $[\hat{R}_i,\hat{P}_j]=0$ for $i\neq j$, we have

$$[\hat{\mathcal{R}},\hat{\mathcal{P}}]=\mu\sum_{k=1}^{A_{\mathrm{tot}}}[\hat{R}_k,\hat{P}_k]. \tag{A2}$$

Using the definitions, Eq. (3), of the operators $\hat{R}$ and $\hat{P}$ it is straightforward to obtain the relation

$$(i\hbar)^{-1}[\hat{R},\hat{P}]=\{s(z-Z_0)\}^2+(z-Z_0)s(z-Z_0)s'(z-Z_0), \tag{A3}$$

where a prime denotes the derivative.

Inserting Eq. (A1) into Eq. (A3) we find for the second term of the RHS of Eq. (A3),

$$\{\mathrm{erf}[a(z-Z_0)]-\eta\}a(z-Z_0)\times\exp\{-a^2(z-Z_0)^2\}/(\sqrt{\pi}2\mu^2)|_{a\to\infty}=0. \tag{A4}$$

Therefore, the uncertainty commutation relation corresponds to

$$\begin{aligned}(i\hbar)^{-1}[\hat{\mathcal{R}},\hat{\mathcal{P}}]-1&=-1+\mu\sum_{k=1}^{A_{\mathrm{tot}}}[s(z_k-Z_0)]^2\\&=\frac{2\eta}{1-\eta^2}\left\{\eta-\left[A_{\mathrm{tot}}^{-1}\sum_{k=1}^{A_{\mathrm{tot}}}\mathrm{erf}[a(z_k-Z_0)]\right]_{a\to\infty}\right\}\\&=O(\eta^2).\end{aligned} \tag{A5}$$

In the derivation of Eq. (A5) it is taken into account that in a space of square integrable functions the operator $A_{\mathrm{tot}}^{-1}\Sigma_{k=1}^{A_{\mathrm{tot}}}(\{\mathrm{erf}[a(z_k-Z_0)]\}^2-1)_{a\to\infty}=0$. It is worth noticing here that an expectation value of the RHS of Eq. (A5) vanishes since the term $(A_{\mathrm{tot}}^{-1}\{\Sigma_{k=1}^{A_{\mathrm{tot}}}\mathrm{erf}[a(z_k-Z_0)]\}_{a\to\infty})=\hat{\eta}$ represents mass asymmetry operator.

To demonstrate that the operator $\hat{P}$ is Hermitian we consider the difference

$$D=\int_{-\infty}^{+\infty}dx g(x)^*[\hat{P}f(x)]-\int_{-\infty}^{+\infty}dx[\hat{P}g(x)]^*f(x), \tag{A6}$$

where $g(x)$ and $f(x)$ are square integrable functions implying that $g(x)$, $f(x)|_{x\to\pm\infty}=0$. Making use of Eq. (3) and integrating by parts in, e.g., the first term of the difference, Eq. (A6), we obtain the Hermitian equality

$$D=-i\hbar[g(x)^*s(x)f(x)]_{-\infty}^{+\infty}=0. \tag{A7}$$

[1] V. A. Benderskii, V. I. Goldanskii, and D. E. Makarov, Phys. Rep. **233**, 195 (1993).
[2] W. A. Fowler, Rev. Mod. Phys. **56**, 149 (1984).
[3] C. E. Rolfs and W. S. Rodney, *Cauldrons in the Cosmos* (Chicago University, Chicago, 1988).
[4] M. Beckerman, Phys. Rep. **129**, 145 (1985); Rep. Prog. Phys. **51**, 1047 (1988).
[5] R. Vandenbosch, Annu. Rev. Nucl. Part. Sci. **44**, 447 (1992).
[6] W. Reisdorf, J. Phys. G **20**, 1297 (1994).
[7] A. B. Balantekin and N. Takigawa, Rev. Mod. Phys. **70**, 77 (1998).
[8] Proceedings of the International Workshop on ''Heavy Ion Collisions at Near Barrier Energies'' [J. Phys. G **23**, 1157 (1997)].
[9] K. Hagino, N. Takigawa, M. Dasgupta, D. J. Hinde, and J. R. Leigh, Phys. Rev. Lett. **79**, 2014 (1997); K. Hagino, N. Takigawa, and S. Kuyucak, *ibid.* **79**, 2943 (1997).
[10] M. Beckerman, M. Salomaa, A. Sperduto, J. D. Molitoris, and A. DiRienzo, Phys. Rev. C **25**, 837 (1982).
[11] D. Galetti and M. A. Candido Ribeiro, Phys. Rev. C **50**, 2136 (1994); **51**, 1408 (1995).
[12] R. Dutt, T. Sill, and Y. P. Varshni, Phys. Rev. C **54**, 319 (1996).
[13] S. V. S. Sastry, A. K. Mohanty, and S. K. Kataria, Phys. Rev. C **56**, 1516 (1997).
[14] A. Iwamoto, Z. Phys. A **349**, 265 (1994).
[15] M. A. Candido Ribeiro, L. C. Chamon, D. Pereira, M. S. Hussein, and D. Galetti, Phys. Rev. Lett. **78**, 3270 (1997); **79**, 5218 (1997).
[16] A. Iwamoto and J. A. Maruhn, Z. Phys. A **293**, 315 (1979).
[17] J. R. Nix, Nucl. Phys. **A502**, 609c (1989).
[18] V. M. Kolomietz and V. N. Kondratyev, Z. Phys. A **344**, 125 (1992).
[19] G. F. Bertsch and A. Bulgac, Phys. Rev. Lett. **79**, 3539 (1997).

[20] A. Bonasera, G. F. Bertsch, and E. El-Sayed, Phys. Lett. **141B**, 9 (1984); A. Bonasera, Nucl. Phys. **A439**, 353 (1985); Phys. Rev. C **34**, 740 (1986).
[21] G. F. Bertsch and S. Das Gupta, Phys. Rep. **160**, 190 (1988); A. Bonasera, F. Gulminelli, and J. Molitoris, *ibid.* **243**, 1 (1994).
[22] W. Cassing, V. Metag, U. Mosel, and K. Niita, Phys. Rep. **188**, 363 (1990).
[23] A. Bonasera, V. N. Kondratyev, A. Smerzi, and E. A. Remler, Phys. Rev. Lett. **71**, 505 (1993).
[24] V. N. Kondratyev, A. Smerzi, and A. Bonasera, Nucl. Phys. **A577**, 813 (1994); **A583**, 333 (1995).
[25] A. Bonasera and V. N. Kondratyev, Phys. Lett. B **339**, 207 (1994).
[26] A. Bonasera and A. Iwamoto, Phys. Rev. Lett. **78**, 187 (1997); **79**, 3540 (1997).
[27] A. Bonasera, V. N. Kondratyev, and A. Iwamoto, J. Phys. G **23**, 1297 (1997); in *Proceedings of the XVIIth RCNP International Symposium ''Innovative Computational Methods in Nuclear Many-Body Problems,''* edited by H. Horiuchi *et al.* (World Scientific, Singapore, 1998), p. 492.
[28] V. N. Kondratyev and A. Iwamoto, Phys. Lett. B **423**, 1 (1998).
[29] V. N. Kondratyev and M. Di Toro, Phys. Rev. C **53**, 2176 (1996); V. N. Kondratyev, Phys. Lett. A **190**, 465 (1994); Z. Phys. B: Condens. Matter **99**, 473 (1996).
[30] W. U. Schröder and J. R. Huizenga, in *Treaties on Heavy-Ion Science*, edited by D. A. Bromley (Plenum, New York, 1984), Vol. 2, p. 114.
[31] A. K. Jain and N. Sharma, Phys. Rev. C **24**, 1066 (1981).
[32] G. F. Bertsch, Z. Phys. A **289**, 913 (1978).
[33] J. M. Negele, Rev. Mod. Phys. **54**, 913 (1982); Phys. Today **38**, 24 (1985).
[34] D. M. Brink, *Semi-Classical Methods for Nucleus-Nucleus Scattering* (Cambridge University, Cambridge, England, 1985).
[35] C. Y. Wong, Phys. Rev. Lett. **31**, 766 (1973).
[36] A. B. Balantekin, S. E. Koonin, and J. W. Negele, Phys. Rev. C **28**, 1565 (1983); M. Inui and S. E. Koonin, *ibid.* **30**, 175 (1984).
[37] M. Dasgupta, A. Navin, Y. K. Agarwal, C. V. K. Baba, H. C. Jain, M. L. Jhingan, and A. Roy, Phys. Rev. Lett. **66**, 1414 (1991).
[38] A. B. Balantekin, A. J. DeWeerd, and S. Kuyucak, Phys. Rev. C **54**, 1853 (1996).
[39] A. Iwamoto and P. Möller, Nucl. Phys. **A596**, 329 (1996); **A605**, 334 (1996).
[40] E. P. Wigner, Phys. Rev. **40**, 749 (1932); M. Hillery, R. F. O'Connell, M. Scully, and E. P. Wigner, Phys. Rep. **106**, 121 (1984).
[41] R. Machleidt, in *Advances in Nuclear Physics*, edited by J. W.Negele and E. Vogt (Plenum, New York, 1992), Vol. 19, p. 189.
[42] P. Carruthers and F. Zachariesen, Rev. Mod. Phys. **55**, 245 (1983).
[43] S. John and E. A. Remler, Ann. Phys. (N.Y.) **180**, 152 (1987).
[44] C. Jarzynski and G. F. Bertsch, Phys. Rev. C **53**, 1028 (1996); G. F. Bertsch, P.-G. Reinhard, and E. Suraud, *ibid.* **53**, 1440 (1996).
[45] A. Iwamoto, V. N. Kondratyev, and A. Bonasera, in *Tours Symposium on Nuclear Physics III*, edited by M. Arnould, AIP Conf. Proc. No. 425 (AIP, New York, 1998), p. 222.
[46] S.-C. Wu and C. A. Barnes, Nucl. Phys. **A422**, 373 (1984).
[47] G. Royer and B. Remaud, J. Phys. G **9**, 1103 (1983); G. Royer, C. Piller, J. Mignen, and Y. Raffray, *ibid.* **16**, 1077 (1990); G. Royer and C. Piller, *ibid.* **18**, 1805 (1992).
[48] G. Royer and B. Remaud, Nucl. Phys. **A444**, 477 (1985).
[49] R. Bass, Nucl. Phys. **A231**, 45 (1974).
[50] A. Iwamoto and K. Harada, Z. Phys. A **326**, 201 (1987).
[51] R. Schicker *et al.*, Phys. Lett. B **206**, 9 (1988).
[52] D. Ackermann *et al.*, Nucl. Phys. **A609**, 91 (1996).